Journal of Infection and Public Health 14 (2021) 577–587

Contents lists available at ScienceDirect

Journal of Infection and Public Health

journal homepage: http://www.elsevier.com/locate/jiph

Antimicrobial and anticancer properties of *Carica papaya* leaves derived di-methyl flubendazole mediated silver nanoparticles

Sandhanasamy Devanesan[a], Murugesan Jayamala[b], Mohamad S. AlSalhi[a,*], Sankaran Umamaheshwari[b], Amirtham Jacob A. Ranjitsingh[c,*]

[a] Department of Physics and Astronomy, College of Science, King Saud University, Riyadh 11451, Saudi Arabia
[b] Department of Biotechnology, Manonmaniam Sundaranar University, Tamilnadu, India
[c] Department of Biotechnology, Prathyusha Engineering College, Chennai 602025, India

ARTICLE INFO

Article history:
Received 28 December 2020
Received in revised form 8 February 2021
Accepted 14 February 2021

Keywords:
Bioactive compound
Green synthesis
XRD
SEM
TEM
Apoptosis
Western blot

ABSTRACT

Background: In this study, a biologically active molecule, di-methyl flubendazole isolated from the extract of *Carica papaya* leaves confirmed by using GC–MS, ^{1}H NMR, and ^{13}C NMR analysis was applied to synthesize silver nanoparticles (AgNPs). The AgNPs with plant sources an alternative therapeutic agent for synthetic compound used in cancer chemotherapy.
Methods: The AgNPs were characterized using UV, FT-IR, XRD, FESEM with EDX and TEM. The antibacterial effects of AgNPs were determined with agar well diffusion method. The MTT assay used to evaluate the inhibitory effect cell lines. The acridine orange and ethidium bromide and DAPI have used cell morphological effects.
Results: The AgNPs were mono-crystalline and their size ranged from 7 to 22 nm. AgNPs showed good antibacterial activity against both Gram-positive and Gram-negative bacteria. Studies on the antiproliferative potential of bioinspired AgNPs in cancer cell lines revealed that the antiproliferative effect was much stronger in HepG2 than in MCF-7 and A549 cell lines. Similarly, AgNPs exerted less cytotoxic activity in Vero cells (normal cells). AgNPs-treated cells showed necrosis, apoptotic morphology evidenced by cell shrinkage, membrane blebbing, cell decay, and necrosis. HepG2 cells treated with biosynthesized AgNPs exhibited a G0/G1 phase (52–53.37%) blockage. Compared to the control, AgNP-treated HepG2 cells showed elevated ®-actin levels; however, Bcl-2 was significantly down regulated in AgNP-treated cells, indicating the involvement of Bcl-2 in apoptosis.
Conclusion: Overall, the fact that di-methyl flubendazole-based silver nanoparticles showed a novel and cost-effective natural antitumor and antibacterial agent.

Introduction

Nanotechnology and its offshoot nanomedicine are believed to provide several solutions in the health care field. The synthesis of nanoparticles (NPs) from biological matter is an eco-friendly and inexpensive approach. The small size of NPs promotes their applicability in therapeutic uses. Due to their size-dependent properties, metal NPs with a small range can be used to enhance applications in electronics, optoelectronics, magnetic, biomedical, and information storage systems [1,2]. Silver nanoparticles (AgNPs) also have versatile applications, such as in the detection of the presence of pollutant line metals [3,4].

The biosynthesis of NPs has advantages over the chemosynthesis of nanoparticles. The rich availability of biotic materials, such as plants, favors their usage in NPs synthesis without affecting the ecosystem [5,6]. The involvement of the primary and secondary metabolites of plants in the redox reaction during NPs synthesis further supports their usability in NPs synthesis. Biosynthesized NPs have been reported to remediate oxidative stress, genotoxicity, and apoptosis [7,8].

In the biosynthesis of NPs using plants, the phytochemical constituents present in the plants, enzymes, proteins, alkaloids, flavonoids, terpenoids, and other cofactors and capping agents mediate the synthesis of NPs. The biosynthesis of NPs does not require any specific culturing or conditions that are required for microbes involved in NPs synthesis. As plant, products are natural and chemical-free, their utilization in the biosynthesis of NPs is safe and ecofriendly [9,10]. In the present approach, the

* Corresponding authors.
E-mail addresses: malsalhi@ksu.edu.sa (M.S. AlSalhi), ranjitspkc@gmail.com (A.J.A. Ranjitsingh).

https://doi.org/10.1016/j.jiph.2021.02.004

medicinal plant with nutritive fruit *Carica papaya* chosen to synthesize the silver nanoparticles. The silver nanoparticles synthesized using the leaves of *C. papaya* showed anticancer effect by affecting the cell cycle and cause apoptosis in human prostate cancer cells [11] Green synthesis of Iron oxide nanoparticles synthesized using the leaves of *C. papaya* are reported to have dye degradation activity and antibacterial activity [12,13]. The silver nanoparticles synthesized using the peel of papaya exhibited good antibacterial activity against pathogenic *Escherichia coli* and *Staphylococcus aureus* [14]. Regarding the application of *C.papaya* for the biogenesis of nanomedicine particles, all parts of the tree are used. The nanoparticles synthesized using the latex of *C.papaya* moderated silver nanoparticles exhibit good antimicrobial and anticancer applications [15]. The bioactive compounds present in the leaves of C. papaya are explores by several workers including our team. Among the different bioactive compounds, methyl flubendazole found to dominate. Therefore, a study proposed to utilize the compound methyl flubendazole to synthesize silver nanoparticles. The biomedical importance of flubendazole in the abatement of worm infection, treatment for different types of cancer, and microbial infections has been well-documented [16–20].

In the present study, we demonstrate an innovative way to synthesize AgNPs using the biologically active molecule di-methyl flubendazole and characterized by using the UV, FT-IR, XRD, FE-SEM with EDX and TEM analyses.To the best of our knowledge, this is the first report on the anticancer activity of AgNPs synthesized using the biologically active molecule, di-methyl flubendazole.

Material and methods

Materials

All the chemicals were purchased from Sigma-Aldrich, Mumbai, Tamil Nadu, India. The glassware was acid washed and Autoclaved. Fresh leaves of the fruit yielding plant *C. papaya* were collected from a six months old tree in an organic farm in Tamil Nadu, India. The species was identified using the knowledge of botanists and authenticated in the Department of biotechnology PEC Chennai [PEC bio/21/2019].

Preparation of plant extracts

The fresh and healthy leaves of *C. papaya* were washed repeatedly with running tap water to remove any dirt and dust, then washed with DH_2O and shade-dried at room temperature (26 ± 2 °C) for 10–15 days. Then the leaves were coarsely powdered using a pulverizer. From the leaf powder, 100 g was extracted using a Soxhlet apparatus with different solvents, such as petroleum ether, chloroform, ethyl acetate, methanol ethanol, and water, to determine the presence of phytochemicals. The leaf powder was extracted until the solvent became colorless in the thimble, after which it was filtered using Whatmann No.1 filter paper. The resulting residues were stored in amber-colored glass vials at 4 °C until further use. The preliminary phytochemical analysis revealed that methanol extraction yielded a good amount of different compounds.

Compound isolation

The crude extract obtained was further subjected to column one thin layer chromatography. A total of 50 fractions was obtained in TLC for fractionalization the solvent hexane: chloroform: methanol was used in the ratio 6:5:3 0.2 ml. The fractions that showed an Rf value of 0.89–4.095 were further selected. These fractions were colored vital for further study. The fractions were further purified using TLC and the fraction with the Rf value 0.895 was further dried and crystallized. This faction was subjected to ^{1}HNMR and ^{13}C NMR studies. Based on the NMR study the isolated compound in the fraction was identified to a dimethyl flubendazole. The compound was stored for further study.

Synthesis and characterization of AgNPs

For the synthesis of AgNPs, ten milligrams of the biologically active molecule di-methyl flubendazole was mixed with 10 ml of Milli Q water and filtered using a syringe filter (0.2 μm). About 3 ml of this compound mixture was added to 97 ml of 0.01 mM $AgNO_3$ solution. The synthesized AgNPs were studied using UV–vis spectroscopy. The dried pellets were further studied using FTIR, XRD, SEM, and TEM. The size of the synthesized NPs was calculated using the Debye Scherrer equation.

Anti-bacterial activity

The pure clinical isolates used in this study (*Acinetobacter baumannii*, *E. coli, Bacillus subtilis, Klebsiella pneumoniae*, *Salmonella typhi*, and *S. aureus*) were obtained from IMTECH (Chandigarh) and maintained in nutrient agar (NA) slants before use. The antibacterial assay was evaluated using the pathogenic organisms with the well diffusion method with different doses include 25, 50, 75, and 100 μg/ml. A control well was filled with distilled water. The Petri plates were incubated at 37 °C for 48 h.

Cytotoxic effect of synthesized AgNPs

The cytotoxicity of the synthesized AgNPs to normal cells was estimated using MTT assay according to Mosmann [21]. The Vero cell lines were obtained from NCCS, Pune, India. For the MTT assay 96 well flat bottom, culture plates were used. Vero cells at a dose level of 1×10^4 cells were carefully transferred to each well. With the well different concentrations of AgNPs 1–100 μM were added. After that 10 μl of MTT reagents were added to each well and allowed to react for 4 h at 37 °C. After 4 h the reagent was removed and 100 μl of DMSO was added and incubated the plates for 20 min. After incubation, the optical density of the cells in the plates was measured using an ELISA reader.

Calculation of IC_{50} value

The IC_{50} dose is the concentration of the testing material that can inhibit 50 percent of the cell activity under *in vitro* conditions. The IC_{50} can be calculated by plotting the x–y and fit the data with a straight line, using the following equation:

$Y = a * X + b$

Antiproliferative activity of AgNPs

Cell proliferation assay

For the evaluation of the effect of the synthesized AgNPs on tumor cells the following cell lines HepG2, MCF 7, and A549 cell lines were obtained from ATCC and were maintained in DMEM containing 10% of PBS with 100 μg/ml penicillin and 100 μg/ml streptomycin supplements. The cultures were incubated at 37 °C in a humidified atmosphere with 5% CO_2. The effect of AgNPs on the proliferation of cancer cell lines was assessed MTT assay. The MTT assay was carried out as per Mossam [21] protocols. In a 96 well flat bottom culture plate Hep G2, and MCF-7 cell lines were seeded at a density of 1×10^4 cells/ well and incubated at 37 °C for 24 h. After the incubation different concentrations of AgNPs [10−100 μm] were added and followed by Ref. [1].

Study of Morphological changes and Observations of nuclear damage

The analysis of cell morphological changes was evaluated by Ref. [22]. The nuclear morphology of apoptotic cells was observed

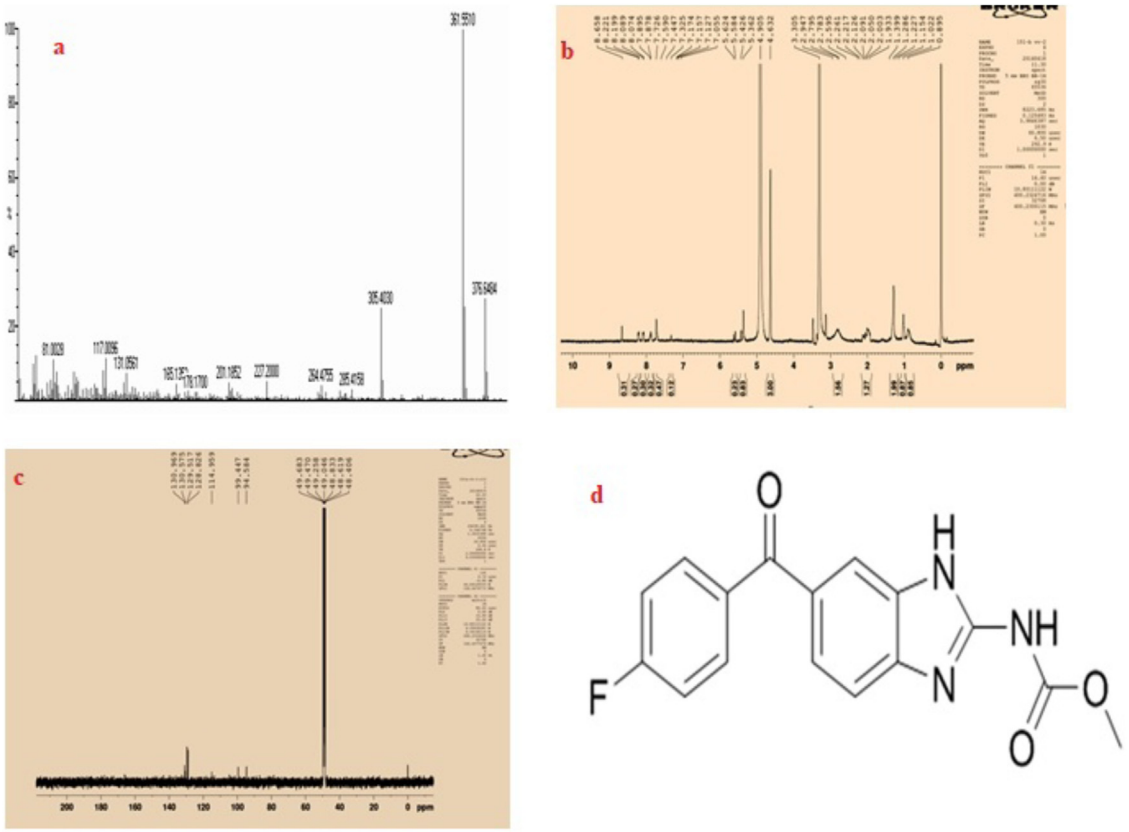

Fig. 1. Gas chromatogram (a), ^{1}H NMR (b), and ^{13}C NMR spectrum (c) of di-methyl flubendazole (d).

using the DAPI. The cell fixation was performed using 37% of paraformaldehyde for ten minutes for laboratory conditions. Then washed with PBS 3 times and absorbed in 0.1% of Triton X-100 for two minutes. The cells were stained with DAPI (10 μg/ml) under low light conditions for 10 min. Later staining, the cellular morphology was observed using a fluorescence microscope.

AO/EB staining for apoptosis study

For studying the morphological changes in the treated cell lines, the dyes acridine orange and ethidium bromide were used [23]. For apoptosis study, the cell lines Hep G2, MCF 7, and A549 were cultured as it is given for cell proliferation assay using different concentrations of AgNPs (10.0, 25.0, and 50.0 μg/ml). After incubation of the cell culture for 48 h at 37 °C, the cells were washed with PBS. The pellets were then centrifuged at 10,000 rpm for five minutes and again suspended in PBS. The cells were stained with AO and EB. For AO/EB dye preparation equal amount (100 μg/ml) of AO and EB were taken and 1 μl of this stain mixture was examined using a fluorescence microscope.

Flow cytometer measurement of cell proliferation

The cell apoptosis was measured by flow cytometry [24]. For apoptosis assay, Hep G2 was chosen. As given in cell proliferation assays, an overnight culture of the HepG2 cells was treated with different doses of AgNPs in 96 wells plates. After treatment and incubation for 24 h at 37 °C. The cells were harvested using PBS. The harvested cells were centrifuged at 10,000 rpm for 10 min. The cells were again washed with PBS and fixed in 70% ethanol for 2 h at -20 °C. After fixation, the cells were washed and suspended in 300 μl PBS and incubated for 30 min at 37 °C.

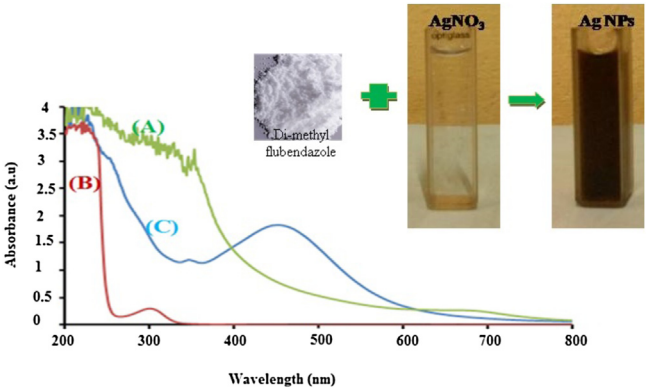

Fig. 2. UV spectrum of (a) di-methyl flubendazole, (b) $AgNO_3$, and (c) synthesized AgNPs from di-methyl flubendazole.

Western blot analysis

The changes in expression of apoptosis-related proteins in HepG2 cells exposed to AgNPs (IC_{50} - 62.68 μg/ml) for 12–48 h at 37 °C were investigated using western blot analysis. Firstly, whole-cell lysates were prepared [25]. After treatment, the cells were harvested and washed with PBS two times before lysing with a mixture of 50 mM of Tris–HCl (pH 8.0), 150 mM of NaCl, 1% Triton X100, 100 μg/ml of phenylmethyl sulfonyl fluoride (PMSF), and 1 μg/ml of aprotinin. After 30 min of incubation using ice, the lysed cells were centrifuged at 10,000 rpm for 15 min at 4 degrees. The total protein concentration was evaluated the protein 50 μg/lane separated on a 10% SDS gel electrophoreses. The protein was shifted onto a nitrocellulose membrane at 20 V, 120 mA for 1.5 h. Gel blocking was performed with 3% skimmed milk overnight at 4 degrees

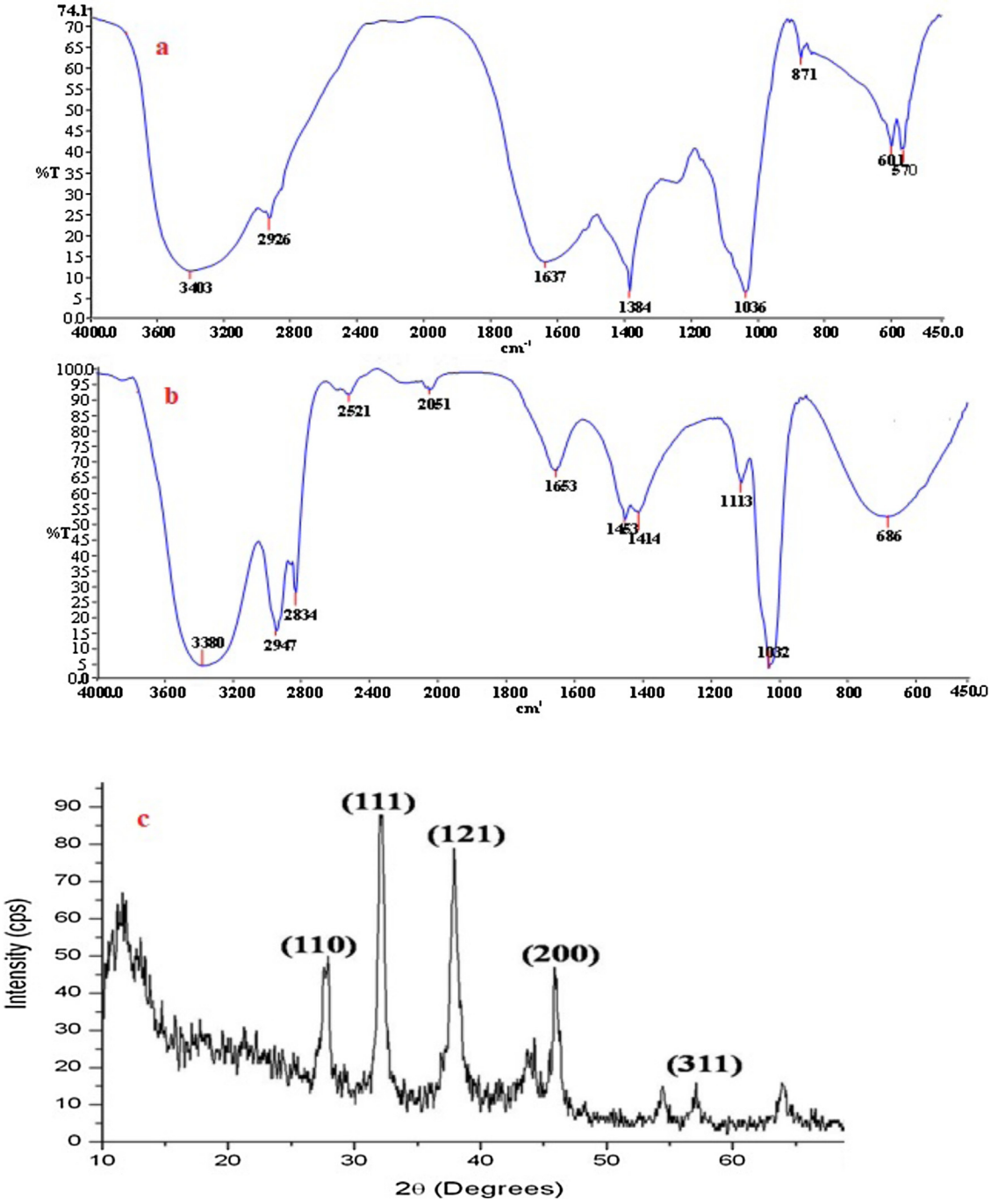

Fig. 3. FT-IR spectrum of (a) di-methyl flubendazole (b) synthesized AgNPs from di-methyl flubendazole and (c) XRD pattern of silver nanoparticles synthesized using di-methyl flubendazole.

and membrane washed with PBS for 5 min before adding the primary antibodies at the respective concentrations of. The antigen BSA 1% and Tween- 20 for 0.1 % were mixed in the PBS. This mixture was incubated for 1 h with gentle rocking. The antigen-antibody complex was washed with PBS for 10 min. To the secondary antibody dose at a dilution of 1:5000, 1% BSA and 0.1 % tween20 was hybridized without disturbing it for 1 h at comfort zone. The bound enzyme activity was detected using a chromogenic substrate NBT-BCIP for visualization under chemiluminescence.

Three independent experiments were performed, and untreated cells were used are constant. Then the cells were unique fluorescent properties analyzed by fluorescence-activated cell sorters.

Arithmetical examination

The experiment for each assay was done thrice and the mean value with standard deviation was calculated. For multiple comparisons, each value was compared using one-way ANOVA. Data with a p-value < 0.05.

Results

The results demonstrated that the biologically active molecule di-methyl flubendazole was isolated from the extract of *C. papaya* leaves by GC–MS, ^{1}H NMR, and ^{13}C NMR analysis. The ESI-MS chromatogram displayed characteristic peaks at 79.2%, correlating with

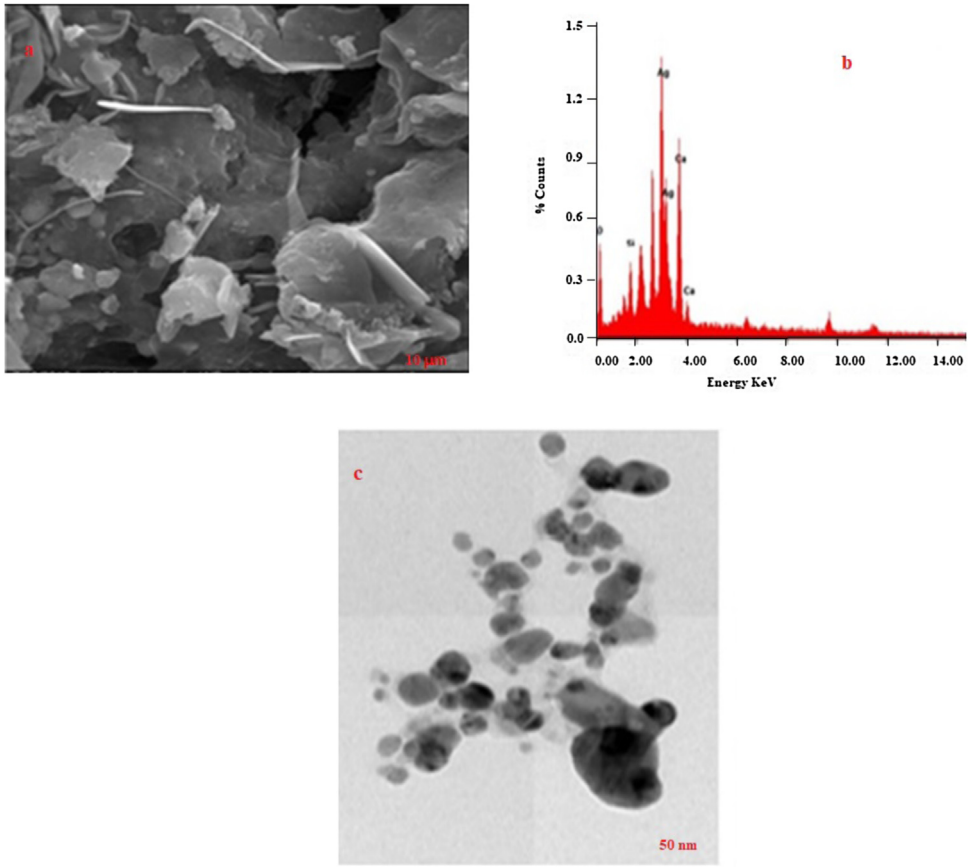

Fig. 4. FE-SEM (a) EDX (b) and HR-TEM (c) analysis of AgNPs synthesized using di-methyl flubendazole.

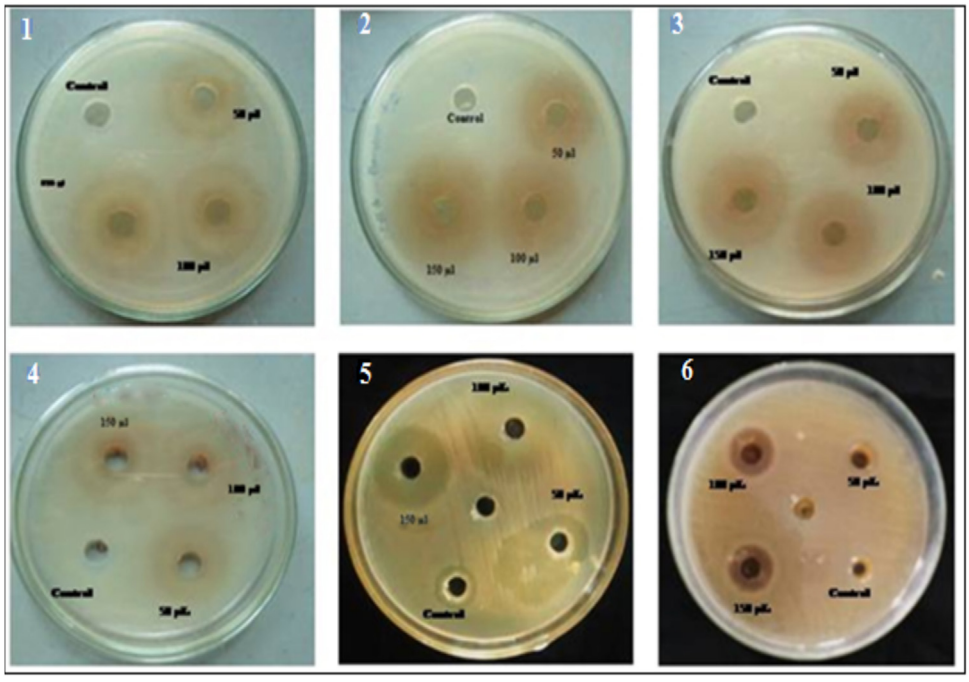

Fig. 5. Antibacterial activity of silver nanoparticles synthesized using di-methyl flubendazole: (1) *A. baumannii*, (2) *B. subtilis*, (3) *E. coli*, (4) *S. aureus*, (5) *K. pneumoniae*, and (6) *S. typhi.*

the MS library data for di-methyl flubendazole. H NMR: 0.874, 0.831, 1.81, 1.17, 1.04, 1.0 (6 s, 20 H, 6 × M), and 2.28. Multiple t-signals between δ 1.40 and δ 1.35 represent the methylene protons on C-7, C-11, and C-15. The multiplet-signals at δ 1.30 to δ 1.00 were assigned to protons on C-6, C-8, C-9, C-10, C12, C-13, C-14, C-16, and C-17 (Fig. 1a–c). Based on the spectral studies, the

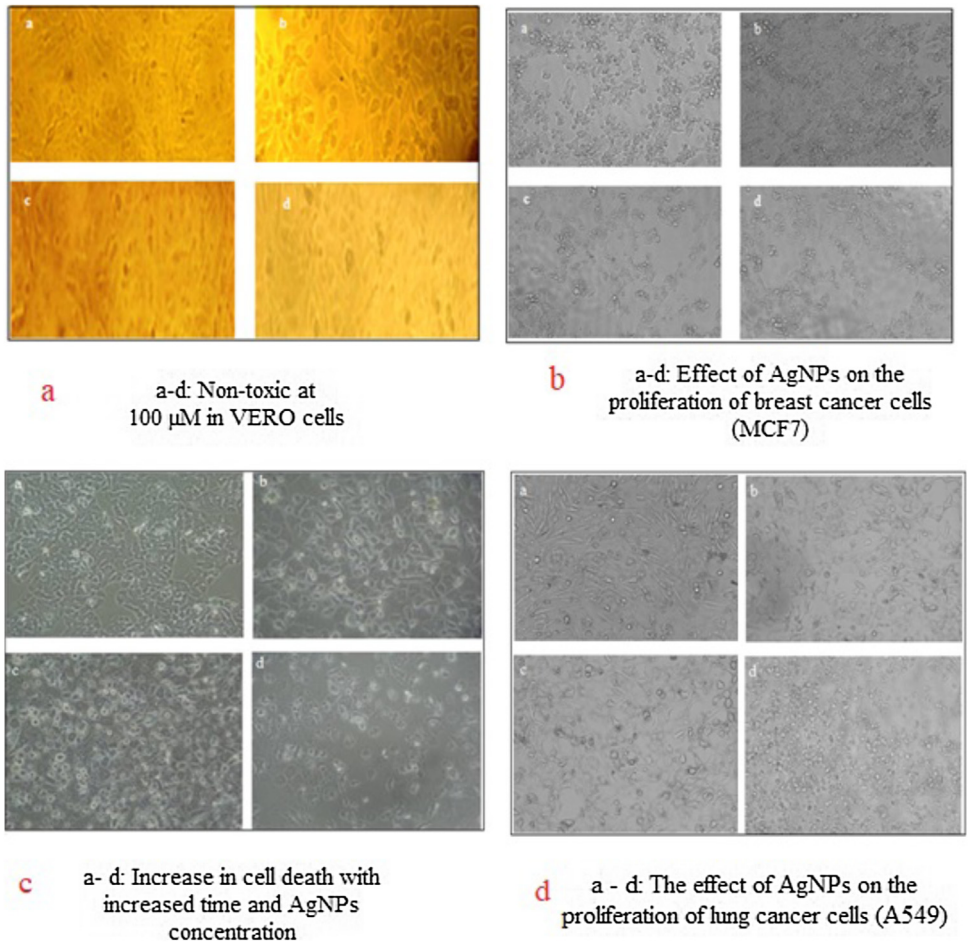

Fig. 6. Antiproliferative activity of silver nanoparticles synthesized using di-methyl flubendazole on VERO cells (a), MCF-7 cells (b), HepG2 cells (c), and A549 cells (d).

active fraction appears to be an extension of di-methyl flubendazole with the molecular formula $C_{16}H_{12}FN_3O_2$, which was confirmed as di-methyl flubendazole (Fig. 1d).

The synthesis of AgNPs was based on observing reaction mixture from light yellow to reddish-brown indicated the formation of AgNPs. UV–vis absorption spectrum peak at 450 nm confirmed the synthesis of AgNPs. (Fig. 2a–c). The major functional groups of the bioactive compound (di-methyl flubendazole) were observed in the FTIR spectrum, including peaks at 3403 cm^{-1} (OH stretch, H-bonded), 2926 cm^{-1} (CH), 1637 cm^{-1} (NH— bend), and 1036 cm^{-1} (C—N stretch) (Fig. 3a). The existing major functional groups in the bioactive compound acted as reducing agents of Ag^+ to Ag°. Synthesized AgNPs showed major functional groups at 3380 cm^{-1} (NH stretch), 2947 $cm—^{-1}$ (CH— stretch), 2834 cm^{-1} (O—H stretch), 2521 cm^{-1} (OH— stretch), 1653 cm^{-1} (—CC stretch), 1453 $cm=^{-1}$ (CC stretch), 1032 $cm—^{-1}$ (CN stretch), and 686 $cm—^{-1}$ (CB—r stretch). The FTIR analysis indicated the peak around at 3380 cm^{-1} corresponded to NH— stretching, and at 2834 cm^{-1} to the O—H stretching and vibrations of phenols and carboxylic acids (Fig. 3b). These components are aldehydes, ketones, carboxyl, and hydroxyls. Under acidic conditions, Ag^+ bound to the biomolecules containing carboxyl and hydroxyl to generate complexions. Then, the aldehydes and ketones reduced Ag^+ ions to AgNPs and became oxidized to carboxyl ions. Using this method, the molecules were strongly adsorbed onto the surface of the AgNPs.

The characteristic Bragg's reflections can be observed in the XRD pattern shown in Fig. 3c. The peaks at the 2θ degrees of 36.1, 48.66, 61.10, and 75.69. The crystalline planes corresponded to the (111), (121), (200), and (311) FCC of the metallic nanoparticles obtained. The crystal size of the AgNPs was calculated using XRD, which suggested that the size were 6–71 nm. The main peaks may be due to the presence of bioactive compounds.

The FESEM and EDX allowed further characterizing the nanoparticles. The FESEM images exhibited the presence of spherical structures of AgNPs with an average size of approximately 12−28 nm. EDX analysis suggested that the phytochemicals were absorbed on the surface of the AgNPs and are responsible for the stability of the biosynthesized nanoparticles (Fig. 4a). HRTEM analysis of the biosynthesized AgNPs was spherical with a moderate variation in particle size due to the functional groups present in the bioactive compound. According to the size of the distribution, most of the AgNPs ranged between 7 and 22 nm (Fig. 4b). The AgNPs were monocrystalline and could be observed using selected area electron diffraction (Fig. 4c).

The antibacterial features of the biosynthesized AgNPs were determined by the agar well diffusion method. The results demonstrated that the AgNPs had antibacterial activity against both Gram-positive and negative bacteria (*A. baumannii*, *B. subtilis*, *E. coli*, *K. pneumoniae*, *S. aureus*, and *S. typhi*). AgNPs exhibited a maximum zone of inhibition against Gram-negative bacteria rather than Gram-positive bacteria when compared to the control. The zone of inhibition of the AgNPs was found to be concentration-dependent (Fig. 5). Among the tested bacteria, *E. coli* responded well to treatment with AgNPs at 100 μg/ml (29 mm), followed by *A. baumannii* (26 mm), *B. subtilis* (25 mm), *K. pneumoniae* (21 mm), and *S. aureus* (18 mm), with the smallest zone of inhibition obtained for *S. typhi* (13 mm). These results indicate that the biosynthesized nanoparticles were efficient on both Gram-positive and negative organisms.

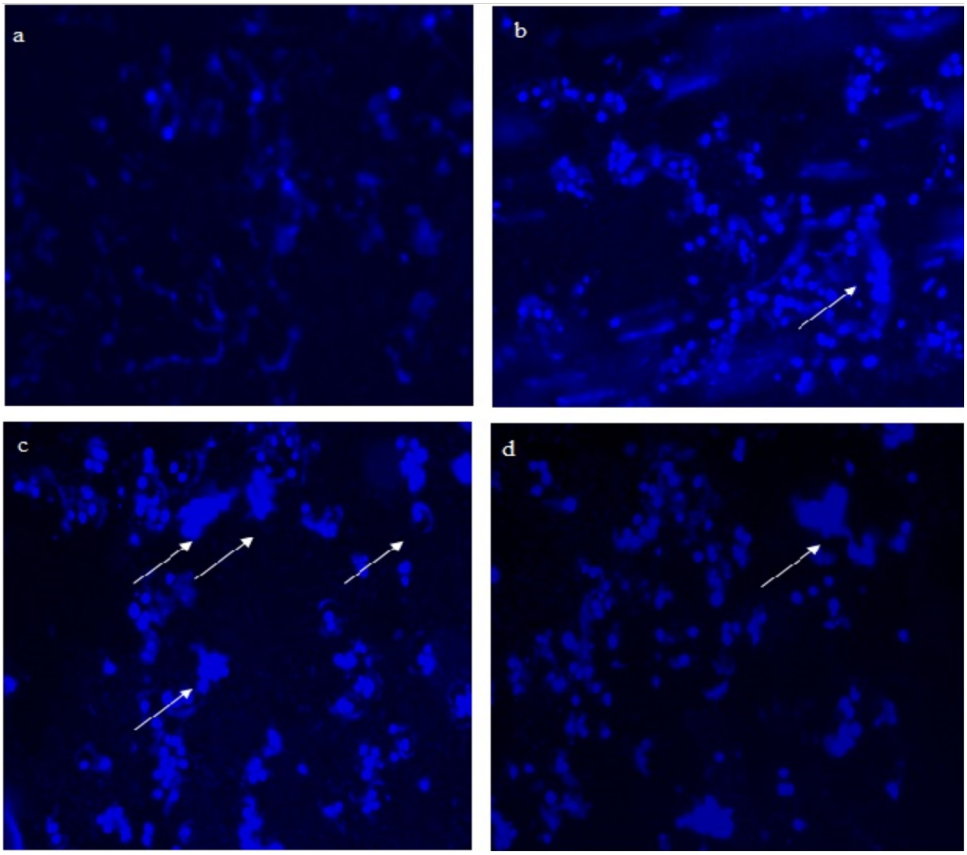

Fig. 7. Apoptotic cell death of HepG2 cells using the DAPI staining method.

The MTT assay was used to evaluate the inhibitory effect of bioactive compound-loaded nanoparticles on various cell lines. The antiproliferative effect of biosynthesized nanoparticles was investigated by treating A549, HepG2, MCF-7 cancer cell lines with AgNPs for different durations (24–48 h). The effects of AgNPs on the proliferation of these cell lines are shown in Fig. 6a–d. It was exhibited that AgNPs exerted a time-dependent antiproliferative effect in HepG2, MCF-7, and A549 cells, which were observed to have IC_{50} values of 45.85, 51.37, and 62.08 μM/ml, respectively. The antiproliferative effect of the HepG2 cell lines was found to be much stronger than that of the MCF-7 and A549 cell lines. The antiproliferation in HepG2 cells increased with time and the maximum activity was observed at 24 h of incubation in all the cell lines.

The biosynthesized nanoparticle-induced morphological changes in HepG2 cells leading to cell death. It has recommended that the AgNPs can be cytotoxic to the cells. The number of dead cells was found to increase with increasing time and AgNPs concentration (Fig. 7a–d). To determine whether the cells died due to apoptosis, the cells were stained with diamidino-2-phenylindole and nuclear morphology changes were observed using microscopy (Fig. 7a–d). The control cells were not found any changes morphologically, while the AgNP-treated cells showed necrosis, cell shrinkage, and cell decay.

After treatment with different AgNPs (45.85 μM for 24 h), HepG2 cells showed prominent apoptotic morphology resulting from cell shrinkage, membrane blebbing, and necrosis. The cells in the control group showed normal cell morphology and were green in color (Fig. 8a–d). In the early phases of apoptosis, the cells became yellow with the condensation or fragmentation of chromatin material. In the later phases of apoptosis, the cells become orange in color with apoptotic bodies. Here, the orange-colored cell nuclei developed necrosis with no condensation of chromatin. AO/EB staining also confirmed the early stages of the necrotic event in the AgNP-treated cell lines. After treatment with AgNPs, no abnormal changes were observed in the VERO cells. The size, shape, and structure of the VERO cells treated with AgNPs appeared normal. On the other hand, the treatment of the other cell lines for 24 h resulted in early apoptosis.

After assessing apoptosis, the cell cycle distribution was analyzed after the treatment of cells with bioactive compound-loaded nanoparticles (45.85 μM) for 12–24 h (Fig. 9a–c). After incubating the HepG2 cells with the AgNPs, an apparent accumulation of cells in the G_0/G_1 phase (52–53.37%) at 24 h of incubation was observed. In the absence of AgNPs, MCF-7 and HepG2 cells were found to grow as an asynchronous population in all phases of the cell cycle. After 48 h exposure, the relative number of cells with G_0-G_1 phase DNA decreased, while the population of cells showed a steady decrease in G2-M, and the number of cells dwindled marginally in S phase.

Western blot analysis was carried out to examine whether the bio-nano particles obtained from di-methyl flubendazole upregulate or downregulated apoptotic and anti-apoptotic proteins. After 12 and 24 h of incubation, the HepG2 cells showed an upregulation of ®-actin protein levels compared to the control (Fig. 9b). However, the levels of Bcl-2 protein were significantly downregulated in these AgNP-treated cells. Compared to the control cells, the AgNP-treated HepG2 cells showed an increased concentration of pro-caspase 9, which is essential for the activation of pro-caspase3. Biosynthesized nanoparticles induced a common apoptosis pathway, which is considered the most important feature of malignant tumors. These findings suggest that mitochondrial signaling does not have a major role in AgNP-induced apoptosis. The involvement of caspase played a major role in apoptosis.

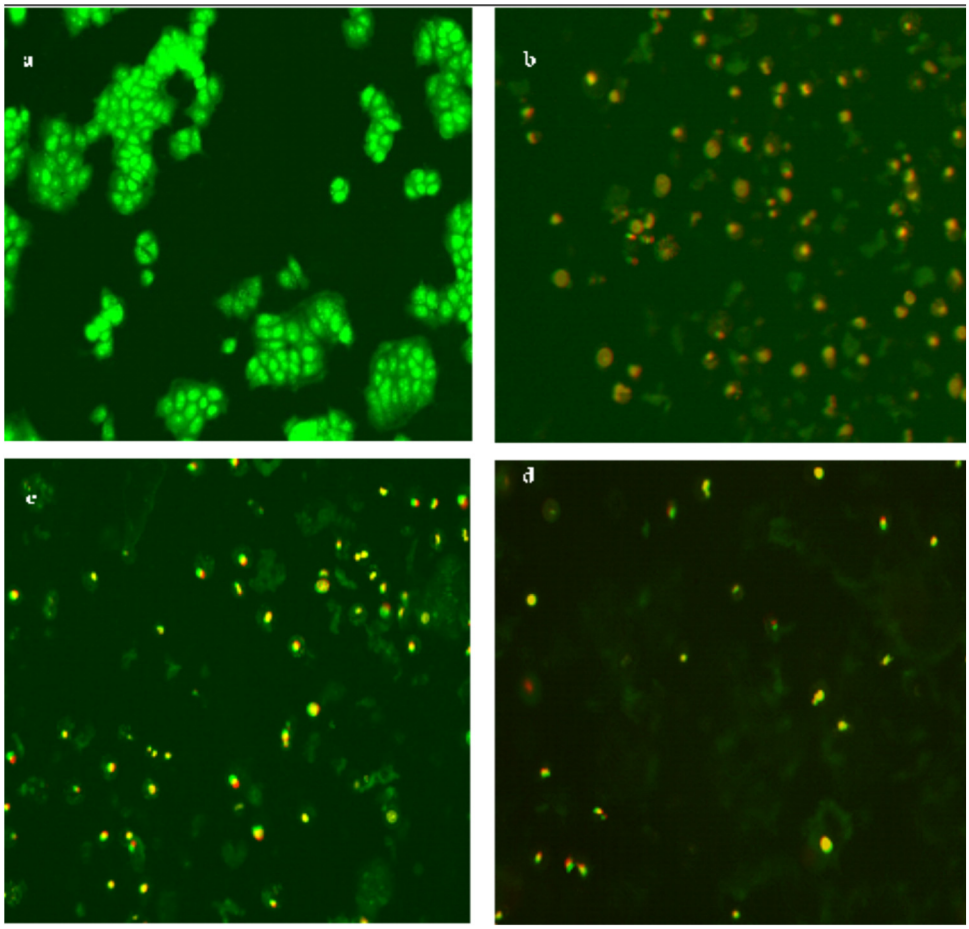

Fig. 8. AgNPs-induced apoptotic cell death in HepG2 cells. (a) Living cells with normal green nuclei. (b, c, d) Apoptotic cells showed orange-stained nuclei with chromatin condensation, while necrotic cells appear with uniformly orange-stained cell nuclei.

Discussion

Nanoparticles involve refining the compatibility and bioavailability of natural products involves the treatment of different cancers [26]. Green synthesis results in well-defined and size-controlled nanoparticles, which prevent contaminants and easy to scale-up [27]. Previously, Firdhouse and Lalitha [28] reported the reduction of Ag^{+} to Ag^{0} using the ethanol extract of leaves of *Pisonia grandis* at room temperature, elevated temperatures, and under sonication conditions. In the synthesis, AgNPs by plant bioactive compounds forms an external biomatrix around the nanoparticles. This biomatrix promotes the binding of drugs to the nanoparticles to enhance the target-oriented delivery of drugs. As the green synthesized nanoparticles are capable of capping, there is no need to incorporate any additional capping or stabilizing agents, resulting in a more cost-effective synthesis of NPs [28].

The antibacterial action of NPs and their ability to deliver drugs to targeted sites have revolutionized the biomedical and pharmaceutical fields. This alternative strategy can provide a remedial measure to contain the development of drug-resistant microbial pathogens, particularly Gram-negative microorganisms [29]. In the spectral assay, no SPR band was observed in the $AgNO_3$ solution or plant compound extracts. The conversion of silver ions into AgNPs can be vividly observed due to the intensity of the spectrum [30]. The spectrum of the IR peak at 3403 cm^{-1} corresponded to the O—H functional group [31], another at 2130 cm^{-1} corresponded to the C—H vibrational mode [32].

The XRD pattern was produced that of AgNPs in our experiments, which was confirmed with the standard method, as evidenced by the peaks at the 2θ values of 27.68°, 38.40°, 42.76°, 46.32°, and 68.68°, correlate to 110, 111, 121, 200, and 220 facets of the face-centered cubic crystalline structure. The finding peaks are evident for particles were presented in nano-regions [33]. The size of the NPs correlated with its ability to penetrate the cells: the smaller the size, the greater the penetration potency, as observed by Morones et al. [34]. Furthermore, it was reported that the morphology of the NPs aids in the execution of damage over target cells. NPs with sharp vertexes and edges can exert more damage to the targeted cells. The synthesized NPs were observed using SEM, and were found to be small and spherical in size. Furthermore, SEM analysis showed that different ranges of NPs due to the aggregation of nanoparticles.

The TEM images were confirmed the spherical nature of the NPs and moderate variations in size. It has been reported that NPs with sizes between 10 and 52 nm are effective for targeting specific sites. Selected area electron diffraction (SAED) analysis confirms the crystalline morphology of the NPs [35].

The action of NPs on bacterial pathogens also depends on their concentration and size. Although large NPs have a broader area for attachment to bacterial pathogens, the smaller NPs are more likely to exhibit a higher percentage of interaction with bacterial cells than their larger counterparts [36]. Nanoparticles with a size of 25 nm have been reported to show a superior antibacterial activity [9,37].

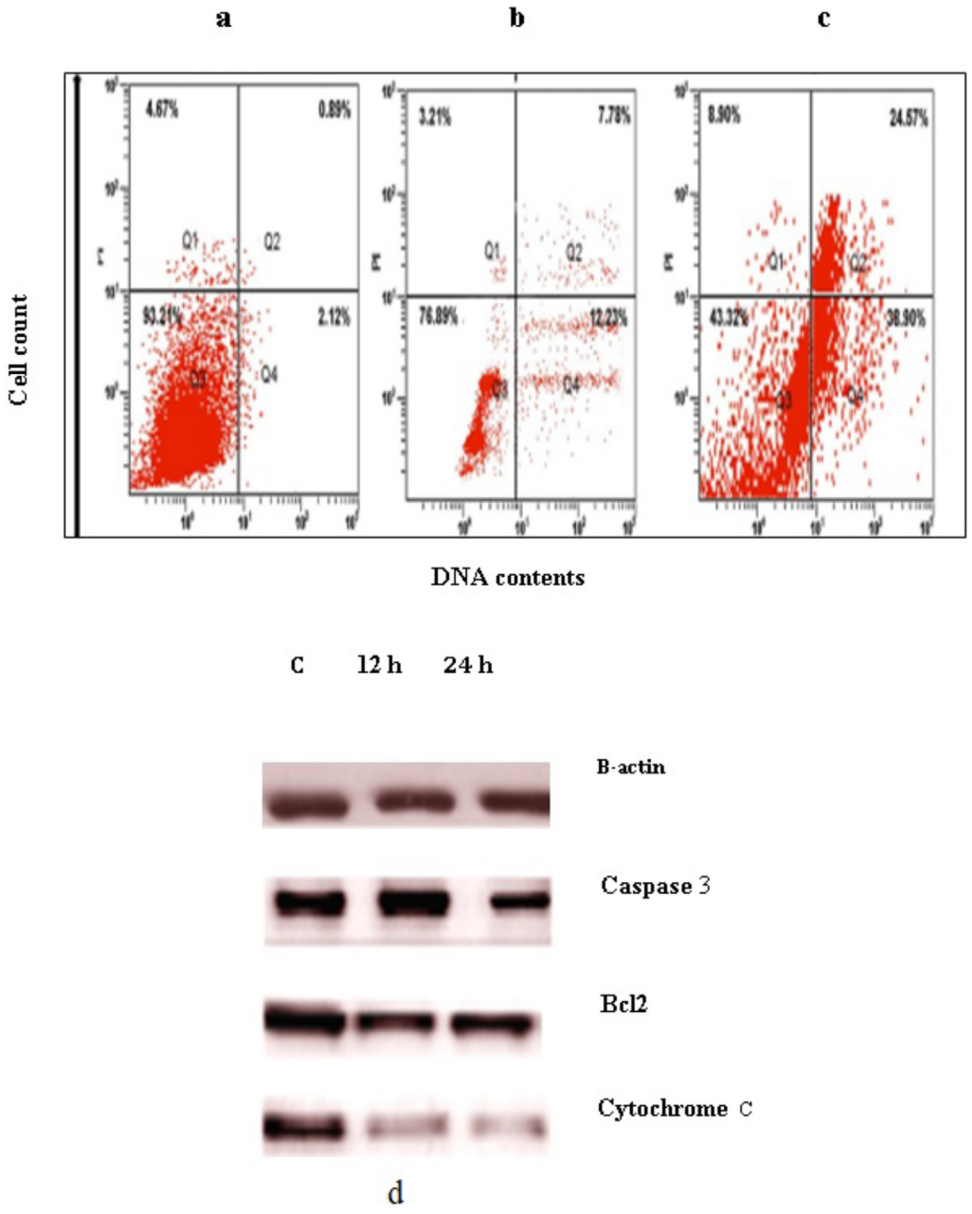

Fig. 9. Cell cycle analysis by flow cytometry of PI-stained HepG2 cells. (a) Control, (b) Ag NPs-treated HepG2 cells (12 h), (c) Ag NPs-treated HepG2 cells (24 h) and (d) Western blot analysis of silver nanoparticle-treated HepG2 cells.

Microbes with antibacterial potential or drug resistance pose a major challenge to the development of cost-effective antibiotics. This is a global concern as alternatives to antibiotics may have to be developed due to the latter's loss of action against microbial pathogens [38].

Dose-dependent cytotoxicity was observed in AgNP-treated MCF-7 cells. An IC_{50} value of biosynthesized AgNPs against MCF-7 cells was found in 10 μg/ml at 24 h and 30 μg/ml at 48 h. The anti-proliferative activity of AgNPs was evaluated against MCF-7 cell lines and it was exhibited to capable to reduce the viability based on the volume-dependent manner. Gurunathan et al. [39], recommended the application of AgNPs as antimicrobial and drug-delivering agents able to kill cancer cells. Despite reports on the antitumor activity of AgNPs, in-depth studies on the changes in the cell architecture are lacking. The mechanisms by which bioactive compounds leading cell death were monitored. Induction of apoptosis leads to morphological alteration, including bulb growth several, cell shrinkage, and n fragmentation [40]. Our findings demonstrated that NPs induced apoptosis in cells, which was identified by AO/EB staining after incubation periods of 24–72 h. Apoptosis was readily identified by cell shrinkage, membrane blebbing, chromosomal condensation, and nuclear fragmentation in lung cancer cells after treatment with sesquiterpene compound [41]. This phytochemical has been reported to show good anticancer activity and antioxidant properties [42,43]. Bioactive compounds have been reported to scavenge ROS and interfere in cell signal transduction pathways and other development for the onset of cancer growth [44,45]. The silver nanoparticles synthesized using biomaterial are found to increase the oxidative stress markers and reducing the antioxidative stress markers. As a result, an upregulation of proapoptotic gene expression takes place. In addition, antiapoptotic gene expression is down-regulated. All the molecular changes due to oxidative stress and subsequent changes in the mitochondrial functioning along with the activation of caspase promote cytotoxicity, and apoptosis [46,47].

Changes in cells, particularly apoptotic degradation, can be measured by analyzing the changes in the DNA during the cell cycle. Studying the cell cycle also helps to detect any DNA fragmentation

or apoptosis development and the activity of cellular endonucleases [48]. During apoptosis, the damaged or excess cells are removed to maintain tissue homeostasis. The cell death process is mediated by surface receptors in the extrinsic pathway, as well as mitochondria and endoplasmic reticulum in the intrinsic pathway [49,50].

Hastemzaei et al. reported the anticancer potential of this bioactive compound when it was found to induce apoptosis in cancer cell lines [40]. Quercetin acted on viable tumor cells and reduced their percentage in a dose-dependent manner, resulting in cell cycle arrest and apoptosis. Caspase, a cysteine protease, functions as a primary effector during apoptosis. It has been reported to proteolytically dismantle most cellular structures, including the endoplasmic reticulum, Golgi apparatus, nucleus and mitochondria [51].

Conclusion

AgNPs were successfully synthesized using a bioactive molecule, di-methyl flubendazole, derived from the *C. papaya*. The synthesized NPs were 7–22 nm in size. The antimicrobial effects showed that a AgNPs was able to act against both Gram-positive and negative organisms. The anticancer effects of the synthesized AgNPs were also evaluated, using three different tumor cell lines, HepG2, MCF-7, and A549, along with a control cell line (Vero cells). Although the synthesized AgNPs showed considerable antiproliferative action against the tested cell lines, the HepG2 cells were the most vulnerable to the action of NPs. The AgNPs-treated HepG2 cells were found to have unregulated β-actin protein levels compared to the control. In conclusion, the cytotoxicity of AgNPs synthesized using a bioactive molecule, di-methyl flubendazole was proven to be efficient for the development of a natural compound for the treatment of cancer.

Funding

No funding sources.

Competing interests

None declared.

Ethical approval

Not required.

Acknowledgment

The authors are grateful to the Researchers Supporting Project number (RSP-2020/68), King Saud University, Riyadh, Saudi Arabia.

References

[1] AlSalhi MS, Devanesan S, Alfuraydi A, Vishnubalaji R, Munusamy MA, Murugan K, et al. Green synthesis of silver nanoparticles using *Pimpinella anisum* seeds: antimicrobial activity and cytotoxicity on human neonatal skin stromal cells and colon cancer cells. Int J Nanomedicine 2016;11:4439–49.
[2] Banerjee P, Satapathy M, Mukhopahayay A, Das P. Leaf extract mediated green synthesis of silver nanoparticles from widely available Indian plants: synthesis, characterization, antimicrobial property and toxicity analysis. Biores Bioproc 2014;1:1–10.
[3] Zhang XF, Liu ZG, Shen W, Gurunathan S. Silver nanoparticles: synthesis, characterization, properties, applications, and therapeutic approaches. Int J Mol Sci 2016;17:1534.
[4] Balavigneswaran CK, Sujin Jeba Kumar T, Moses Packiaraj R, Prakash S. Rapid detection of Cr (VI) by AgNPs probe produced by *Anacardium occidentale* fresh leaf extracts. Appl Nanosci 2014;4:367–78.
[5] Devanesan S, AlSalhi MS, Balaji RV, Ranjitsingh AJA, Ahamed A, Alfuraydi AA, et al. Antimicrobial and cytotoxicity effects of synthesized silver nanoparticles from *Punica granatum* peel extract. Nanoscale Res Lett 2018;13:315.
[6] Alfuraydi AA, Devanesan S, Al-Ansari M, AlSalhi MS, Ranjitsingh AJA. Eco-friendly green synthesis of silver nanoparticles from the sesame oil cake and its potential anticancer and antimicrobial activities. J Photochem Photobiol B 2019;192:83–9.
[7] Kim S, Ryu DY. Silver nanoparticle-induced oxidative stress, genotoxicity and apoptosis in cultured cells and animal tissues. J Appl Toxicol 2013;33:78–89.
[8] Mahassni SH, Al-Reemi RM. Apoptosis and necrosis of human breast cancer cells by an aqueous extract of garden cress (*Lepidium sativum*) seeds. Saudi J Biol Sci 2013;20:131–9.
[9] Devanesan S, AlSalhi MS, Balaji RV, Alfuraydi AA, Alajez NM, Alfayez M, et al. Rapid biological synthesis of silver nanoparticles using plant seed extracts and their cytotoxicity on colorectal cancer cell lines. J Clust Sci 2017;28:595–605.
[10] Khatua A, Priyadarshini E, Rajamani P, Patel A, Kumar J, Naik A, et al. Phytosynthesis, characterization and fungicidal potential of emerging gold nanoparticles using *Pongamia pinnata* leave extract: a novel approach in nanoparticle synthesis. J Clust Sci 2020;31:125–31.
[11] Singh SP, Mishra A, Shyanti RK, Singh RP, Acharya A. Silver nanoparticles synthesized using *Carica papaya* leaf extract (AgNPs-PLE) causes cell cycle arrest and apoptosis in human prostate (DU145) cancer cells. Biol Trace Elem Res 2021;199:1316–31.
[12] Bhuiyan MSH, Miah MY, Paul SC, Aka TD, Saha O, Rahaman MM, et al. Green synthesis of iron oxide nanoparticle using *Carica papaya* leaf extract: application for photocatalytic degradation of remazol yellow RR dye and antibacterial activity. Heliyon 2020;6(8):e04603.
[13] Jain A, Ahmad F, Gola D, Malik A, Chauhan N, Dey P, et al. Multi dye degradation and antibacterial potential of Papaya leaf derived silver nanoparticles. Environ Nanotechnol Monit Manag 2020;14:100337.
[14] Balavijayalakshmi J, Ramalakshmi V. *Carica papaya* peel mediated synthesis of silver nanoparticles and its antibacterial activity against human pathogens. Int J Appl Res Inf Technol Comput 2017;15(5):413–22.
[15] Chandrasekaran R, Gnanasekar S, Seetharaman P, Keppanan R, Arockiaswamy W, Sivaperumal S. Formulation of *Carica papaya* latex-functionalized silver nanoparticles for its improved antibacterial and anticancer applications. J Mol Liq 2016;219:232–8.
[16] Zhou X, Liu J, Zhang J, Wei Y, Li H. Flubendazole inhibits glioma proliferation by G2/M cell cycle arrest and pro-apoptosis. Cell Death Discov 2018;4(18), http://dx.doi.org/10.1038/s41420-017-0017-2.
[17] Chang L, Zhu L. Dewormer drug fenbendazole has antiviral effects on BoHV-1 productive infection in cell cultures. J Vet Sci 2020;21(5):e72.
[18] Zhou X, Zou L, Chen W, Yang T, Luo J, Wu K, et al. Flubendazole, FDA-approved anthelmintic, elicits valid antitumor effects by targeting P53 and promoting ferroptosis in castration-resistant prostate cancer. Pharmacol Res 2020:105305.
[19] Zhen Y, Zhao R, Wang M, Jiang X, Gao F, Fu L, et al. Flubendazole elicits anticancer effects via targeting EVA1A-modulated autophagy and apoptosis in Triple-negative Breast Cancer. Theranostics 2020;10(18):8080–97.
[20] Dogra N, Kumar A, Mukhopadhyay T. Fenbendazole acts as a moderate microtubule destabilizing agent and causes cancer cell death by modulating multiple cellular pathways. Sci Rep 2018;8:11926, http://dx.doi.org/10.1038/s41598-018-30158-.
[21] Mosmann T. Rapid colorimetric assay for cellular growth and survival: application to proliferation and cytotoxicity assays. J Immunol Methods 1983;65:55–63.
[22] Manikandan R, Beulaja M, Arulvasu C, Sellamuthu S, Dinesh D, Prabhu D, et al. Synergistic anticancer activity of curcumin and catechin: an *in vitro* study using human cancer cell lines. Microsc Res Tech 2012;75:112–6.
[23] Liu K, Liu PC, Liu R, Wu X. Dual AO/EB staining to detect apoptosis in osteosarcoma cells compared with flow cytometry. Med Sci Monit Basic Res 2015;9:15–20.
[24] Joel MS. Assaying cell cycle status using flow cytometry. Curr Protoc Mol Biol 2015;111:1–11.
[25] Lavi S, Gaitini D, Milloul V, Jacob G. Impaired cerebral CO_2 vasoreactivity: association with endothelial dysfunction. Am J Physiol Heart Circ Physiol 2006;29:1856–61.
[26] Jeyaraj M, Sathishkumar G, Sivanandhan G, Mubarak Alid D, Rajesh M, Arun R, et al. Biogenic silver nanoparticles for cancer treatment: an experimental report. Colloid Surf B Biointerfaces 2013;106:86–92.
[27] Ullah Khan S, Saleh TA, Wahab A, Khan MHU, Khan D, Ullah Khan W, et al. Nanosilver: new ageless and versatile biomedical therapeutic scaffold. Int J Nanomedicine 2018;13:733–62.
[28] Firdhouse MJ, Lalitha P. Bio synthesis of silver nanoparticles using the extract of *Alternanthera sessilis* anti proliferative effect against prostate cancer cells. Cancer Nanotechnol 2013;4:137–43.
[29] Desselberger U. Emerging and re-emerging infectious diseases. J Infect 2000;40:3–15.
[30] Khalil MMH. Green synthesis of silver nanoparticles using olive leaf extract and its antibacterial activity. Arab J Chem 2013;7:1131–9.
[31] Gajbhiye M, Kesharwani J, Ingle A, Gade A, Rai M. Fungus-mediated synthesis of silver nanoparticles and their activity against pathogenic fungi in combination with fluconazole. Nanomedicine 2009;5:382–6.
[32] Johnson PJM, Koziol KL, Hamm P. Intrinsic phasing of heterodyne-detected multidimensional infrared spectra. Opt Express 2017;25:2928–38.

[33] Dubey SP, Lahtinen M, Sarkka H, Sillanpaa M. Bio-prospective of *Sorbus aucuparia* leaf extract in development of silver and gold nano-colloids. Colloids Surf B Biointerfaces 2009;80:26–33.
[34] Morones JR, Elechiguerra JL, Camacho A, Holt K, Kouri JB, Ramírez JT, et al. The bactericidal effect of silver nanoparticles. Nanotechnology 2005;10:346–53.
[35] Thirunavoukkarasu M, Balaji U, Behera S, Panda PK, Mishra BK. Biosynthesis of silver nanoparticle from leaf extract of *Desmodium gangeticum* (L.) DC. And its biomedical potential. Spectrochim Acta A Mol Biomol Spectrosc 2013;116:424–7.
[36] Paredes D, Ortiz C, Torres R. Synthesis, characterization, and evaluation of antibacterial effect of Ag nanoparticles against *Escherichia coli* O157:H7 and methicillin-resistant *Staphylococcus aureus* (MRSA). Int J Nanomedicine 2014;9:1717–29.
[37] Ashraf A, Zafar S, Zahid K, Salahuddin Shah M, Al-Ghanim KA, Al-Misned F, et al. Synthesis, characterization, and antibacterial potential of silver nanoparticles synthesized from *Coriandrum sativum L.* J Infect Public Health 2019;12:275–81.
[38] Singh J, Dutta T, Kim KH, Rawat M, Samddar P, Kumar P. Green synthesis of metals and their oxide nanoparticles: applications for environmental remediation. J Nanobiotechnology 2018;6:e84.
[39] Gurunathan S, Lee KJ, Kalishwaralal K, Sheikpranbabu S, Vaidyanathan R, Eom SH. Antiangiogenic properties of silver nanoparticles. Biomaterials 2009;30:6341–50.
[40] Yang CS, Landau JM, Huang MT, Newmark HL. Inhibition of carcinogenesis by dietary polyphenolic compounds. Annu Rev Nutr 2001;21:381–406.
[41] Fartha AK, Geetha BS, Nair M. Antineoplastic effects of deoxyelephantopin, a sesquiterpene lactone from *Elephantopus scaber* on lung adenocarvcinoma (A549) cells. J Integr Med 2013;11:269–77.
[42] Middleton E, Kandaswami C, Theoharides TC. The effects of plant flavonoids on mammalian cells: implications for inflammation, heart disease, and cancer. Pharmacol Rev 2000;52:673–751.
[43] Yang Z, Zhou L, Zhou L, Wu LM, Lai MC, Xie HY, et al. Overexpression of long noncoding RNA HOTAIR predicts tumor recurrence in hepatocellular carcinoma patients following liver transplantation. Ann Surg Oncol 2011;18:1243–50.
[44] Krych J, Gebicka L. Catalase is inhibited by flavonoids. Int J Biol Macromol 2013;58:148–53.
[45] Al-Sheddi ES, Al-Zaid NA, Al-Oqail MM, Al-Massarani SM, El-Gamal AA, Farshori NN. Evaluation of cytotoxicity, cell cycle arrest and apoptosis induced by *Anethum graveolens* L. essential oil in human hepatocellular carcinoma cell line. Saudi Pharm J 2019;27:1053–60.
[46] Yuan YG, Zhang S, Hwang JY, Kong IK. Silver nanoparticles potentiates cytotoxicity and apoptotic potential of camptothecin in human cervical cancer cells. Oxid Med Cell Longev 2018;6121328:1–21.
[47] Ferdous Z, Nemmar A. Health impact of silver nanoparticles: a review of the biodistribution and toxicity following various routes of exposure. Int J Mol Sci 2020;21(7):2375.
[48] Elmore S. Apoptosis: a review of programmed cell death. Toxicol Pathol 2007;35:495–516.
[49] Farah MA, Ali MA, Chen SM, Li Y, Al-Hemaid FM, Abou-Tarboush FM, et al. Silver nanoparticles synthesized from *Adenium obesum* leaf extract induced DNA damage, apoptosis, and autophagy via generation of reactive oxygen species. Colloid Surf B Biointerfaces 2016;141:158–69.
[50] Hashemzaei M, Delarami-Far A, Yari A, Heravi RE, Tabrizian K, Taghdisi SM, et al. Anticancer and apoptosis inducing effect of Quecerin in vitro and in vivo. Oncol Rep 2017;38:819–28.
[51] Chen Q, Kang J, Fu C. The independence of and associations among apoptosis, autophagy, and necrosis signal transduction and targeted therapy. Signal Transduct Target Ther 2018;3:18.